RESEARCH

Numerical Investigation on Mechanism Analysis of Bubble Pinch-off

Meng Jia[1] · Mingjun Pang[1]

Abstract

The studies on bubble pinch−off deviates to some degree from the actual situation due to limitations in theoretical assumptions and experimental conditions, and physical details such as satellite bubbles inside the bubble cannot be observed. Even some of the published experimental results are divergent. To fully understand the dynamics of bubble pinch−off, the authors applied the volume of fluid (VOF) method to investigate the effect of liquid−phase viscosity on bubble pinch−off, and analyzed the pinch−off process and the surrounding flow field. It was found that in low−viscosity liquids, the process of bubble pinch−off is relatively fast and the position corresponding to R_{min} varies only in the axial direction; and satellite bubbles during pinch−off shows vertical distribution, which enter the upper and lower parts with the jet after bubble pinch−off. In intermediate and high viscosity liquids, a gas line is formed after bubble pinch−off, and the length and duration of the gas line increase with an increase in liquid−phase viscosity; and the position corresponding to R_{min} moves not only radially inward, but also axially upward. In liquids of different viscosities, the strength of annular flow and the radial pressure drop are different, which leads to different phenomena of bubble pinch−off.

Keywords Bubble generation · Neck pinch-off · Effect of liquid-phase viscosity · Pinch-off mechanism

Introduction

To improve the efficiency of heat and mass transfer between phases, bubbles are widely used as auxiliary media in industrial processes such as biochemicals (Liew and Hlastala 1969), mineral flotation (Theander and Pugh 2004; Rubio et al. 2002), wastewater treatment (Temesgen and Han 2023), and drag reduction by bubbles(García-Magariño et al. 2023; Wang et al. 2020). Bubbles also play an important role in the heat and mass transfer in the natural world such as the ocean (Wang et al. 2023; Han et al. 2023; Han and Chen 2020) and geology(Parmigiani et al. 2016). To improve and control effectively the transfer efficiencies between phases, it is important to study the mechanism of bubble generation to effectively control bubble sizes. Researchers such as Simmons et al. (Simmons et al. 2015), Yang et al. (Yang et al. 2007), and Yuan et al. (Yuan et al. 2014) have investigated the effects of fluid parameters (density, viscosity, wettability, and surface tension), structural parameters (needle

diameter, geometry, and chamber volume), and operational parameters (flow rate and pressure) on the overall characteristics of bubble generation, i.e., the effects of the above parameters on bubble shape, size, and generation time. The related investigations are reviewed in detail by Kulkarni and Joshi (Kulkarni and Joshi 2005) and Jia and Pang (Jia and Pang 2023). It was found that the process of bubble generation involves three stages: nucleation, expansion and necking (Di Bari et al. 2013), of which the duration of the necking process accounts for about one−third of the total generation time. Therefore, it is very important for bubble generation to understand bubble pinch−off. In addition, the pinch−off process in the necking process is a typical singularity phenomenon in the field of nonlinear dynamics due to the infinite increase of stress and pressure, so it is very important. However, the local dynamics of bubble pinch-off have not been well understood due to the short duration (about hundreds of microseconds) and the small neck size (atomic scale). Moreover, the pinch-off process of bubble generation is similar to the fission of subatomic nuclei (Skobelev 2020), the formation of celestial stars (Chandrasekhar 2005) and black holes (Liebling and Choptuik 1996), and the explosion of supernovae (Plewa et al. 2004). Compared to the above exotic phenomena, the study of bubble pinch-off

✉ Mingjun Pang
  pangmj@cczu.edu.cn

[1] School of Mechanical Engineering and Rail Transit,
     Changzhou University, Changzhou 213164, China

is relatively simple and is easy to be performed. A deep study on the neck pinch-off mechanism of bubble generation is also conducive to the understanding of other nonlinear dynamical singularities. A review of bubble pinch-off is presented as follows.

Earlier, the neck pinch-off of droplet generation has been extensively studied (Eggers 1997; Han and Chen 2021, 2019). In references (Leppinen and Lister 2003; Chen and Steen 1997), it is pointed out that the dynamic process of droplet pinch-off is controlled by the local equilibrium between surface tension and inertial force irrespective of viscosity, and the power-law exponent of the curve of the minimum radius of the neck as a function of time is $\alpha = 2/3$. With an increase in the viscosity of droplets, the minimum radius of the neck decreases linearly as a function of time, and then $\alpha = 1$ (Eggers 1993). Under the conditions that the power law exponent is independent of the initial conditions and fluid properties, the droplet pinch-off is self-similar and universal (Bolanos-Jiménez et al. 2009). If the droplet is generated in an external fluid with medium viscosity, the dynamic process of droplet pinch-off depends on the balance between surface tension and viscous force of the two fluids, and inertial effects can be neglected (Lister and Stone 1998). Doshi et al. (Doshi et al. 2003) conducted an experiment in which a droplet is generated inside silicone oil. They summarized that if the external fluid is particularly viscous and the viscosity of the internal fluid (i.e., a droplet) is also large, the droplet develops a long and thin fluid filament before pinch-off, thus breaking universality.

Recently, some experimental and theoretical studies have been carried out on the neck pinch-off process of bubble generation. Longuet-Higgins et al. (Longuet-Higgins et al. 1991) experimentally found that during the bubble pinch-off, an axial jet is formed, which flows upward into the bubble. Burton et al. (Burton et al. 2005) experimentally investigated the bubble pinch-off in liquid and showed that the exponent α is a function of the viscosity of external Newtonian liquids: for low-viscosity liquids ($\mu_l \leq 10$ cP), $\alpha \approx 0.5$ and $R_{min} \propto (r_o \sigma / \rho_l)^{1/4} \tau^{1/2}$; for intermediate-viscosity liquids (10 cP < μ_l < 100 cP), $0.5 \leq \alpha \leq 1$; and for high-viscosity liquids ($\mu_l \geq 100$ cP), $\alpha \approx 1$ and $R_{min} \propto \tau \sigma / 2 \mu l$. Where R_{min} denotes the minimum radius of bubble neck, r_o denotes the radius of the orifice, σ is the surface tension, ρ_l is the liquid density, τ denotes the time difference between any time and the exact moment of pinch-off during the pinch-off process, and μ_l denotes the liquid viscosity. Burton et al. (Burton et al. 2005) observed that when bubbles are generated in high-viscosity liquids, the bubble neck shows a parabolic shape and R_{min} decreases linearly with an increase in τ; when bubbles are generated in intermediate-viscosity liquids, a filament with a radius of 6 μm is formed during bubble pinch-off, and it eventually ruptures into about 50 satellite bubbles; during the bubble pinch-off process in low-viscosity liquids, when

R_{min} decreases to 25 μm, the neck suddenly breaks and two satellite bubbles with a diameter of 10 μm are formed. Keim et al. (Keim et al. 2006) experimentally found that the neck shape of bubble pinch-off in water is very sensitive to initial conditions, and a small tilt angle of the needle destroys the axisymmetry of the neck shape during the bubble pinch-off, and $\alpha = 0.56 \pm 0.03$ at zero tilt angle. Bergmann et al. (Bergmann et al. 2006) experimentally observed the evolution of the surface shape of a huge air cavity when a metal disk drops into a deep pool of water, and found that the power-law exponent is related to the Froude number, and the bubble profile approaches a cylindrical shape quickly as the Froude number increases. Thoroddsen et al. (Thoroddsen et al. 2007) investigated experimentally the neck pinch-off of bubble generation from vertical needles, and found that the power-law exponent for bubble generation with air, helium, and SF6 in water is approximately $\alpha = 0.56$–0.60, which is slightly greater than 0.5. However, in low-viscosity liquids, Thoroddsen et al. (Thoroddsen et al. 2007) did not observe the sudden breakage of bubble neck reported by Burton et al. (Burton et al. 2005). In high-viscosity ($\mu_l = 810$ cP) liquids, air lines are also clearly observed. Burton et al. (Burton et al. 2005) observed that two satellite bubbles formed after bubble pinch-off are radially distributed, whereas Thoroddsen et al. (Thoroddsen et al. 2007) found that they are vertically distributed. Bolaños-Jiménez et al. (Bolaños-Jiménez et al. 2008) experimentally investigated the growth and pinch-off process of bubbles from a vertical needle at the bottom of a pool under quasi-static conditions. It was shown that bubble pinch-off is controlled simultaneously by the capillary force, the hydrostatic pressure difference and the initial velocity of gas, and the duration of bubble pinch-off increases with an increase in needle radius. Bolaños-Jiménez et al. (Bolanos-Jiménez et al. 2009) experimentally and theoretically investigated bubble pinch-off in stationary viscous liquids, focusing on the effect of liquid viscosity on the last moment before bubble pinch-off. It is found that the power-law exponent α in the transition region does not reflect the effect of liquid-phase viscosity well, because α increases from 0.58 to 1 with an increase in Reynolds number during the pinch-off process and the value of α is not accurately defined in the transition region, which cannot be used to characterize the dynamics of bubble pinch-off. Jiang et al. (Jiang et al. 2017) investigated bubble pinch-off in Newtonian and non-Newtonian liquids, respectively. The authors found that the gas-phase flow rate does not affect the value of α, and it is always 0.5 for low-viscosity Newtonian liquids, $\alpha = 0.5$ for medium-viscosity liquids and low surface tension, and $\alpha = 1$ for higher-viscosity liquids. Rajesh et al. (Rajesh et al. 2022) experimentally investigated bubble pinch-off in polymer solutions and analyzed in detail the effect of polymer concentration on the evolution of R_{min} against τ (i.e., the effect of viscoelasticity on bubble pinch-off). The results showed that the

presence of polymer does not affect the pinch-off process until a later stage; however, when the polymer concentration is sufficiently high, the pinch-off process is delayed. Pahlavan et al. (Pahlavan et al. 2019) experimentally investigated bubble pinch-off in microcapillary tube, and it was found that in unbounded basins, the liquid phase flows predominantly along the radial direction during the pinch-off stage of bubble neck. This implies that the axial dimensions of bubble neck are sensitive to the initial experimental conditions, making the pinching process non-universal. However, in the confined region, the axial dimension of bubble neck during pinch-off is not affected by the initial conditions, and thus the pinch-off process is universal.

In addition to experimental studies, some theoretical and numerical ones on bubble pinch-off have been carried out. Eggers et al. (Eggers et al. 2007) derived a power-law exponential law on axisymmetric cavity pinch-off using the slender-body theory $\alpha = 0.5 + 1/[4(-\ln(\tau))^{0.5}]$. Gordillo et al. (Gordillo 2008) presented a model to analyze the axisymmetric bubble pinch-off in a low-viscosity liquid, and presented the criterion $d\ln R_{min} r_1/ds(R_{sat}) = -1$ for the generation of satellite bubbles. Here R_{sat} is the radius of satellite bubbles, r_1 is the axial curvature of bubble neck, and $s = -\ln(R_{min})$. The necessary condition of the formation of tiny satellite bubbles are presented based on theoretical analyses and the maximum velocity of the Worthington jet is predicted. Oguz and Prosperetti (Oguz and Prosperetti 1993) simulated bubble pinch-off in the potential flow using the boundary integral method and confirmed $\alpha = 0.5$ for underwater bubble generation. Suryo et al. (Suryo et al. 2004) numerically investigated the pinch-off of an annular jet, and found that the local shape of neck interface near the pinch-off point is parabolic and pinching is not self-similar. Gordillo et al. (Gordillo et al. 2005) theoretically and numerically investigated bubble pinch-off under potential flow conditions at high Reynolds numbers. It was pointed out that when bubble initial interface is symmetric up and down, the local shape of bubble interface near the singularity is similar to a parabolic shape; if bubble initial interface is asymmetric, the bubble interface near the singularity tends to show the conical shape with different cone angles at the top and bottom. It is also explained that when $\alpha = 1/3$, the final stage of bubble pinch-off is not controlled solely by surface tension or liquid inertia, but by the combined control of liquid and gas inertia. Rodríguez-Rodríguez et al. (Rodríguez-Rodríguez et al. 2006) numerically investigated the pinch-off of droplets and bubbles in high Reynolds number strain flows based on the potential flow theory. It was found that during the bubble pinch-off process, bubble neck oscillates infinitely but does not break when the Weber number (We) is less than a critical value ($We_c = 2.3$), and it always breaks to form two sub-bubbles when $We > We_c$. Gordillo and Fontelos

(Gordillo and Fontelos 2007) theoretically analyzed the importance of gas inertia for bubble pinch-off, and presented the expressions describing the characteristics and dimensions of satellite bubbles. The authors found that the size of satellite bubbles in water depends on the density of gas, and the diameter of satellite bubbles decreases as the gas–liquid density ratio decreases. Garzon et al. (Garzon et al. 2012) numerically investigated bubble pinch-off in a double inviscid fluid system using the coupling of level set and boundary integral methods and reproduced the dynamics of droplet and bubble pinch-off accurately. Albadawi et al. (Albadawi et al. 2013) numerically investigated the bubble generation and detachment process using the volume of fluid (VOF) method and the coupled level set and volume of fluid method (CLSVOF) method, showing $\alpha = 0.36$ at the bubble detachment stage. Oshajhi et al. (Oshaghi et al. 2019) numerically investigated the bubble formation and entrapment processes in shear-thinning liquids at lower capillary and Bond numbers using the VOF method based on the OpenFOAM solver. For the system of water and air, $\alpha = 0.34$ agrees with the result of Albadawi et al. (Albadawi et al. 2013). Chu et al. (Chu et al. 2019) provided the review of recent theoretical and experimental studies on bubble pinch-off. Han et al. (Han et al. 2024) investigates microbubble breakup in microchannels with Vshaped obstacles. Four breakup patterns are identified: no breakup, breakup with permanent gaps, breakup with partly obstruction, and breakup with permanent obstruction. The bubble breakup with permanent obstruction could maintain a wider flow pattern range.

In summary, the current theoretical studies on the neck pinch-off during bubble generation are based on certain assumptions (e.g., potential flows or inviscid fluids), which are somewhat deviated from actual conditions. The experimental studies are limited to shooting conditions and resolution limitations, which cannot achieve the desired results and cannot effectively observe satellite bubbles entering pinched bubbles in low-viscous fluids (Thoroddsen et al. 2007). Moreover, some of the experimental results on bubble pinch-off in low- and high-viscosity liquids are divergent (e.g., in low-viscosity liquids, the reference (Burton et al. 2005) reported the sudden breakage of bubble neck, whereas this phenomenon is not observed in the reference (Thoroddsen et al. 2007); in high-viscosity liquids, the gas line is not observed in the former, whereas it is reported in the latter, and the gas line splits into satellite bubbles). To fully understand the dynamics of bubble pinch-off and obtain mechanism explanations, it is necessary to conduct a more detailed study on this phenomenon. In this paper, the effect of liquid-phase viscosity on bubble pinch-off is thoroughly investigated by direct numerical simulation, and the pinch-off process and the surrounding flow field are analyzed in detail.
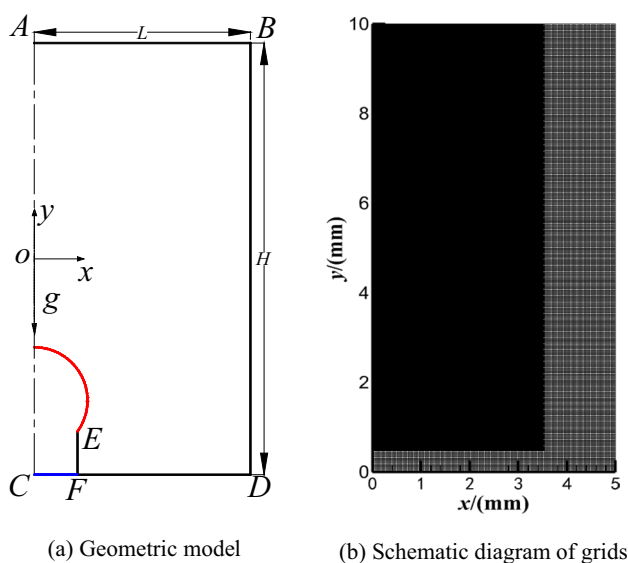
(a) Geometric model

(b) Schematic diagram of grids
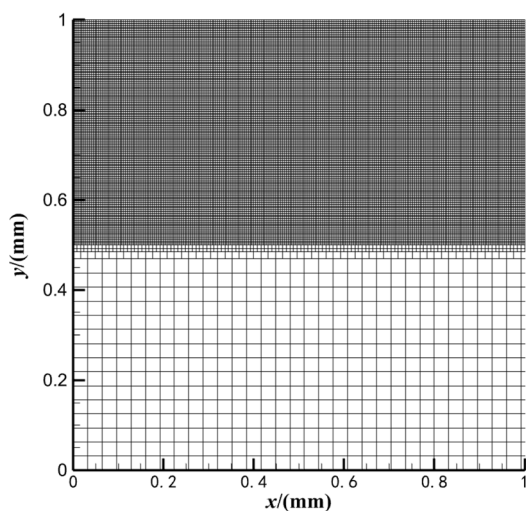
(c) Local enlargement of refined grids

Fig. 1 Geometric model and Schematic diagram of regional refined grids. (**a**) Geometric model. (**b**) Schematic diagram of grids. (**c**) Local enlargement of refined grids

Physical problems and Governing Equations

Geometric Model

To save computational costs, the computational region is simplified into a two − dimensional axisymmetric model, as shown in Fig. 1. A single bubble is generated from the top of a capillary needle with a radius of r_o. To eliminate the influence of the wall effect on bubble generation as much as possible and to ensure the full growth of a bubble in the vertical direction, the model size of L and H are set to $L = 10$ r_o and $H = 20 r_o$. To simulate the generation of a single bubble, the following assumptions are presented: (1) the gas flow rate in a capillary needle is low, and all the gas is used to generate a bubble; (2) the generation of a bubble occurs under a quasi − static condition; (3) the compressibility of fluids is ignored; and (4) the generated bubble is spherical and can be seen as a circle in the two − dimensional axisymmetric model.

Design of Computational Cases

Existing studies have shown that bubble pinch-off is tightly related to the viscosity magnitude of external liquid (Bolanos-Jiménez et al. 2009; Burton et al. 2005; Thoroddsen et al. 2007), fluid density (Leppinen and Lister 2003), verticality of microcapillary tube, and initial conditions (Gordillo et al. 2005). The effect of viscosity of external liquid is particularly significant. For this reason, the effect of liquid-phase viscosity on bubble pinch-off is only investigated here. The specific physical parameters are listed in Tables 1 and 2. The radius of the needle tube is the same as that in reference (Burton et al. 2005), i.e., $r_o = 1.6$ mm. According to the effect of liquid-phase viscosity on bubble pinch-off in reference (Eggers 1993), the viscosity magnitude of external liquid can be classified into three ranges, i.e., low, intermediate, and high viscosity. And it is defined as follows: high viscosity ($\mu_l \gtrsim 100$

Table 1 Computational parameters

Physical parameters	Liquid density ρ_l/ g/m^3	Gas density ρ_g/ kg/m^3	Gas viscosity μ_g/ Pa·s	Orifice radius r_o/ mm	Inlet velocity v_g/ m/s	Surface tension σ/ N/m	Gravitational level g/ m/s^2
value	1000	1.225	1.7894×10^{-5}	1.6	0.1	0.065	9.8

Table 2 Computational cases

Viscosity range	Low viscosity		Intermediate viscosity			High viscosity
μ_l/ Pa·s	0.001	0.005	0.05	0.08	0.1	0.2
Re_μ	2.08×10^6	8.32×10^5	830	325	208	52

cP), intermediate viscosity (10 cP $< \mu_l <$ 100 cP), and low viscosity ($\mu_l \lesssim$ 10 cP). For the present study, $Bo = 4(\rho_l - \rho_g) gr_o^2/\sigma = 0.1543$, i.e., surface tension is relatively important. The overall effect of viscosity can be characterized by the Reynolds number based on the capillary viscous velocity, as shown in Eq. (1).

$$Re_\mu = \frac{2\rho r_o v_\mu}{\mu_l} \left(v_\mu = \frac{\sigma}{\mu_l} \right) \tag{1}$$

Governing Equations

Presently, it is assumed that the flow is adiabatic and axisymmetric, the injection velocity of gas is uniform, and a two−phase flow is formed at the needle top. Both fluids are considered to be mutually impermeable and incompressible Newtonian ones. The continuity and momentum equations are presented by Eqs. (2) and (3).

$$\nabla u = 0 \tag{2}$$

$$\frac{\partial \rho u}{\partial t} + \nabla \cdot (\rho u u) = -\nabla p + \nabla \cdot \mu (\nabla u + \nabla u^T) + \rho g + F_S \tag{3}$$

where u is the velocity vector, m/s; p is the pressure, Pa; g is the acceleration of gravity, m/s^2; ρ is the average density of fluids, kg/m^3; μ is the average viscosity of fluids, Pa•s; t is the time, s; and ∇ is the Hamiltonian operator. F_S is the volume force due to surface tension, N; and it is calculated by Eq. (4).

$$F_S = \sigma k_s \delta \hat{n} \tag{4}$$

where σ is the surface tension coefficient, N/m; and δ is the Dirac distribution function. k_s is the curvature of bubble interface, and $\hat{n}$ is the unit normal vector of the outward direction of the interface, which are calculated by Eq. (5), respectively.

$$k_s = -\nabla \cdot \hat{n} \left(\hat{n} = \frac{n}{|n|} \right) \tag{5}$$

The average density and viscosity of fluids are calculated by Eqs. (6) and (7).

$$\rho = \rho_l(F) + \rho_g(1 - F) \tag{6}$$

$$\mu = \mu_l(F) + \mu_g(1 - F) \tag{7}$$

In Eqs. (6) and (7), F denotes the phase function, which is defined by Eq. (8).

$$F = \begin{cases} 0 & \text{Bubble} \\ 0 < F < 1 & \text{Interface} \\ 1 & \text{Liquid} \end{cases} \tag{8}$$

Interface Capture Method

The VOF method is used to track the volume of fluids in each grid rather than the motion of fluid particles, and thus it has the advantages of easy implementation, simple computation, and high accuracy compared with other methods. For the VOF method, two kinds of fluids share a set of momentum equations, and the volume fraction of each fluid in each cell is tracked in the whole domain. The VOF method utilizes the volume ratio of fluids in each grid (i.e., F) to achieve the goal based on the fact that two or more fluids are not interpenetrating (Yuan et al. 2014). The transport equation of F is presented by Eq. (9)

$$\frac{\partial F}{\partial t} + u \cdot \nabla F = 0 \tag{9}$$

Interface Reconstruction

Since F is not explicitly related to a specific grid for the VOF method, an algorithm is needed to reconstruct bubble interface. There are several methods to solve the volume function of fluids, such as the donor−acceptor method, the flux line−segment model for advection and interface reconstruction method, the simple line interface calculation method, and the piecewise linear interface calculation method (PLIC) (López et al. 2004). The PLIC method takes into account the transfer of fluids between adjacent interfaces in detail, and thus the reconstruction results are relatively accurate. Therefore, the PLIC method is applied to interface reconstruction here. For the PLIC method, the interface in each cell is approximated by a straight line defined by $n \cdot x + C = 0$, where n and x are the outward unit vector normal to the interface and the position vector of a generic point on the line, respectively, and C is a constant(López et al. 2004).
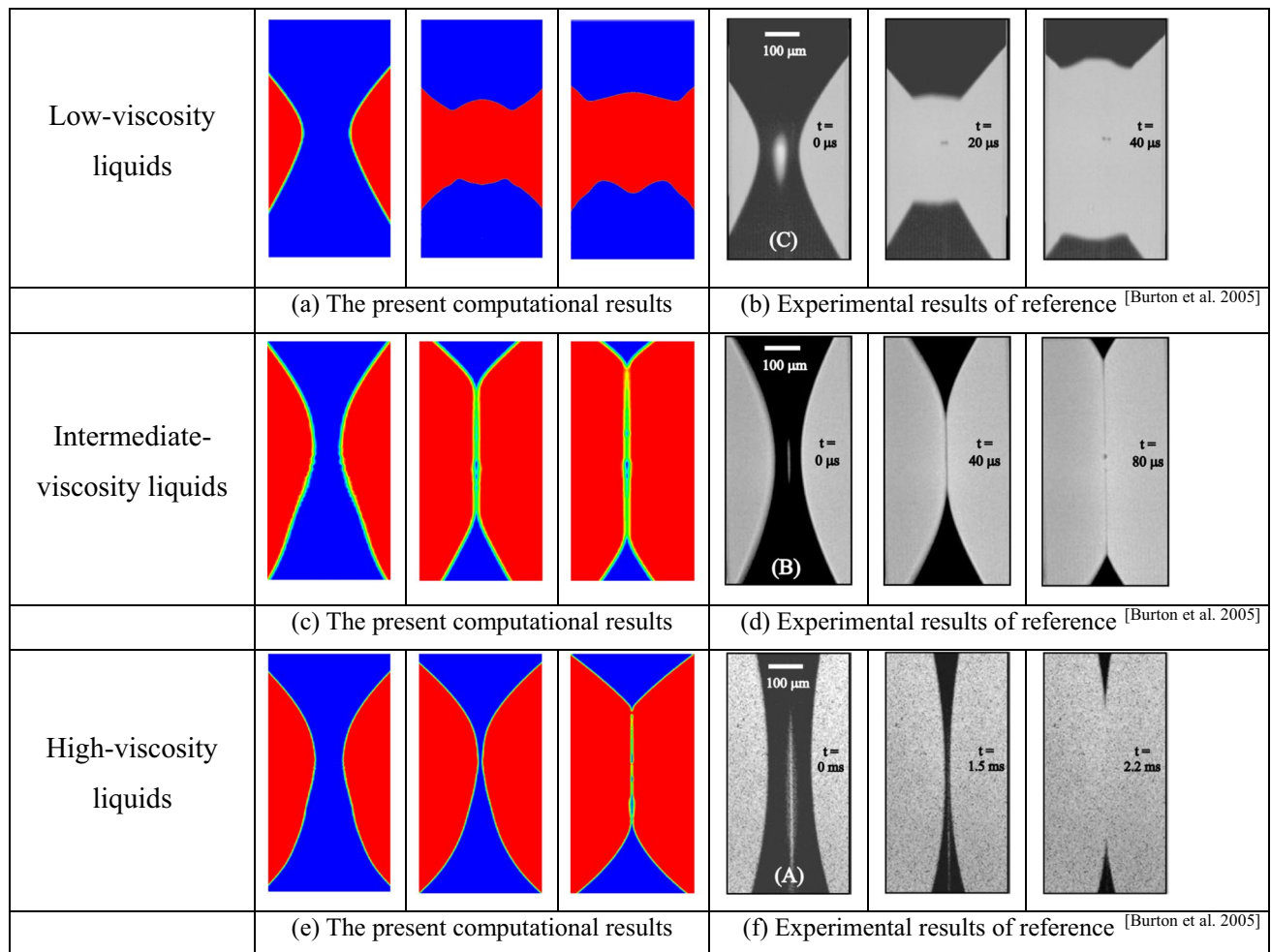
Numerical Methods

For the present calculation, the velocity inlet is applied to CF, the no−slip wall is applied to EF, DF, and BD, the pressure outlet is applied to AB, and the line of AC is the symmetrical axis. Compared with the unstructured grid, the structured grid can be quickly generated, it is easy to fit the boundary of the calculation region, and it has the advantages of good grid quality, high calculation accuracy, and easy calculation convergence(Ma et al. 2012). Therefore, the structured grid is applied to the present computation. To

reduce the computation cost, the region adaption method is used to refine the region containing the bubble, as shown in Fig. 1(b). Referring to the minimum resolution of the camera used by Keim et al. (Keim et al. 2006), the minimum grid size is selected as 4 µm. There are 400 nodes at the location of tube mouth after the refinement, as shown in Fig. 1(c); and there are about 3.35 million grids in the whole computational domain. The coupling between pressure and velocity fields is achieved by the SIMPLE algorithm. The pressure and momentum terms are discretized using the staggered pressure PRESTO and the second−order windward schemes, respectively. Time is advanced with a first-order implicit scheme. Time step is variable, the global Courant number is 0.25, and correspondingly the minimum time step is 10^{-8} s. Before the calculation starts, the initialization is performed so that the calculation domain is filled with stationary liquid, and the needle tube is filled with gas. Then, the two−phase flow calculation starts.

Results and Discussion

Validation of Result Accuracy

To verify the accuracy of computational results, the experimental condition of the reference (Burton et al. 2005) is selected as the verification case. At present, the viscosity values corresponding to the calculated results are $\mu_l = 0.0009$, 0.0374 and 0.2 Pa·s, and other parameters are shown in Table 1. The results are scaled in the same proportion as shown in Fig. 2. It can be seen from Fig. 2 that the calculation results are basically consistent with those of the reference, showing that the simulation results are approximately accurate and credible. The numerical results are slightly different from those of the reference because the inlet velocity and surface tension are not specified in the reference (Burton et al. 2005).

Low-viscosity liquids	(a) The present computational results	(b) Experimental results of reference [Burton et al. 2005]
Intermediate-viscosity liquids	(c) The present computational results	(d) Experimental results of reference [Burton et al. 2005]
High-viscosity liquids	(e) The present computational results	(f) Experimental results of reference [Burton et al. 2005]

Fig. 2 Verification of result accuracy. (**a**) The present computational results. (**b**) Experimental results of reference(Burton et al. 2005). (**c**) The present computational results. Experimental results of reference(Burton et al. 2005). (**e**) The present computational results. (**f**) Experimental results of reference (Burton et al. 2005)

Analysis of Pinch-off Process

During the growth of a bubble, the gas flows out of the needle at a constant flow rate. And at the expansion stage, the bubble grows in a quasi-static manner, and then a neck is formed near the needle, which is pinching. Due to the self-accelerating nature of the neck, the neck continues to contract until the bubble detaches from the top of the needle. (Bolanos-Jiménez et al. 2009). Figure 3 shows the pinch-off process of bubble neck in different viscous liquids. It can be seen that the phenomenon of neck pinch-off occurs in all viscosity liquids. When bubble necks just appear, bubble necks show an asymptotic parabolic shape. As time goes on, bubble necks, which approximate an asymptotic parabolic shape, contract towards the axis. In intermediate- and high-viscosity liquids, after the pinch-off of bubble neck, both the upper and lower parts show a conical shape, similar to the results in references (Thoroddsen et al. 2007; Gordillo 2008). And the magnitude of the cone angle does not change with the liquid-phase viscosity magnitude within a certain viscosity range. As shown in Fig. 3, when the liquid-phase viscosity is large, the cone angle is constant and equal to 90°, which is consistent with the experimental results of reference (Thoroddsen et al. 2007). In low-viscosity liquids, the cone angles of the upper and lower parts are not equal after the pinch-off of bubble neck, and the cone angle of the upper part is relatively large. This is similar to the numerical results of bubble pinch-off in low-viscosity liquids in reference (Leppinen and Lister 2003). It can be seen from the time it takes for bubble pinch-off that an increase in liquid viscosity leads to a longer time for bubble pinch-off. The most significant effect of an increase in liquid viscosity is to delay the pinch-off process. In addition, it can also be seen from Fig. 3 that the tips of the upper and lower conical parts spring back quickly in low-viscosity liquids within a short time after pinch-off. In contrast, in intermediate- and high- viscosity liquids, the tips of the upper and lower conical parts continue to remain conical without significant shape oscillations. This is because the viscous force effectively offset the excess surface energy released by bubble pinch-off, and this buffering effect increases with an increase in the viscosity of the external liquid (Jiang et al. 2017).

In high-viscosity liquids (i.e., $\mu_l = 0.1$ and 0.2 Pa·s), bubble neck gradually decreases to a gas line with a constant radius (about 4 μm) during the pinch-off process. The greater the liquid-phase viscosity is, the longer the gas line is. After the complete pinch-off, the gas line breaks and upper and lower parts with a sharp end form. The present phenomenon is similar to the results of Thoroddsen et al. (Thoroddsen et al. 2007). And the pinch-off time of bubble neck is longer in a more viscous liquid. This is because the more viscous the external liquid is, the greater the viscous drag acting on the bubble is, and the greater its resistance to the pinch-off of bubble neck is. This delays bubble pinch-off (Jiang et al. 2017).
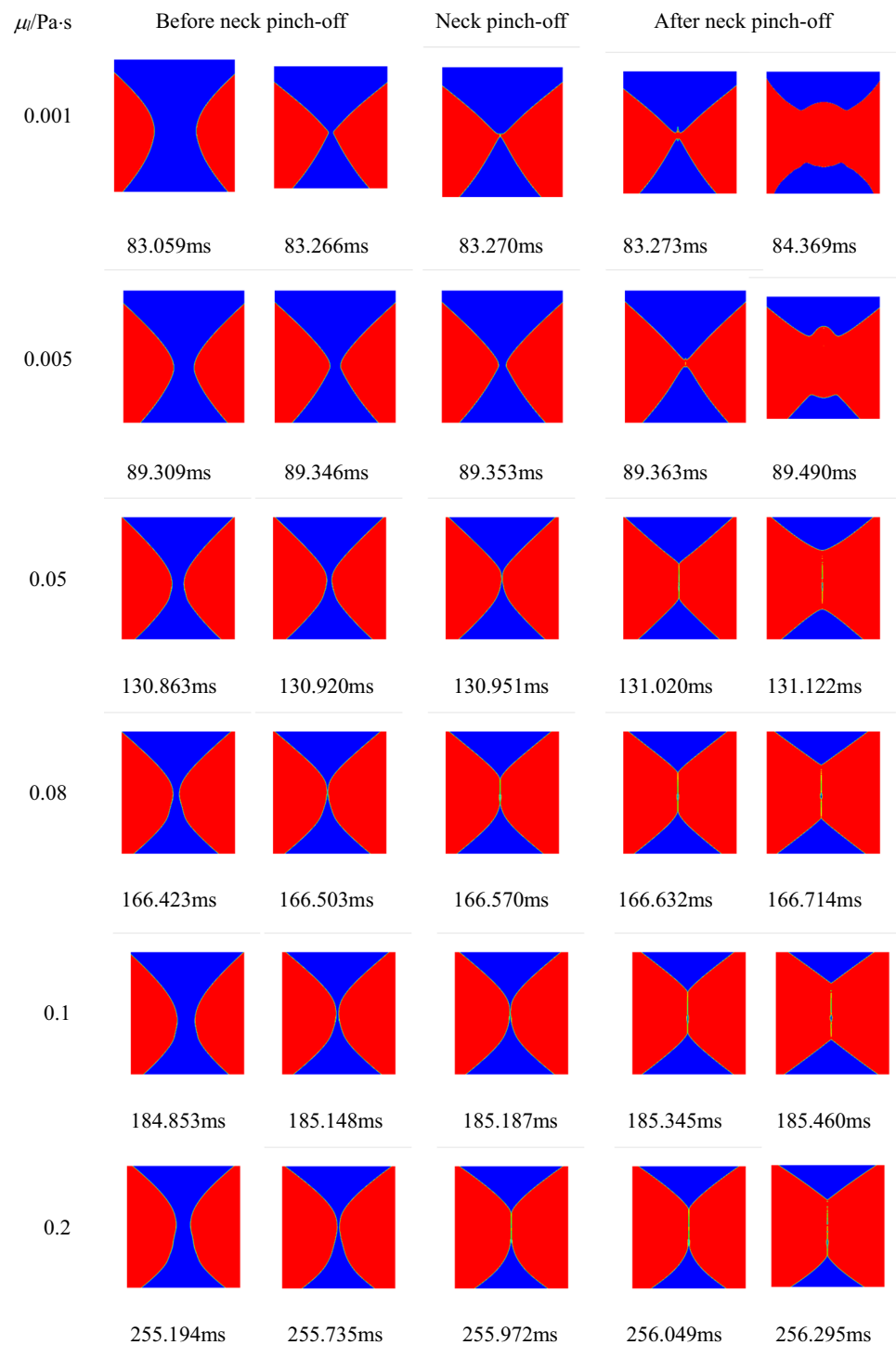
In intermediate-viscosity liquids (i.e., $\mu_l = 0.05$ and 0.08 Pa·s), bubble neck also decreases to a gas line with a constant radius of about 4 μm during the pinch-off process. There is a similar law to high-viscosity liquids. Namely, the higher the liquid viscosity is, the longer the gas line is, and the longer the pinch-off time is. The cone angle of corresponding parts after bubble neck pinch-off is smaller in liquids with a higher viscosity. The present results are slightly different from the experimental results of Burton et al. (Burton et al. 2005), in which the radius of the gas line before breakup is 6 μm in intermediate-viscosity liquids.

In low-viscosity liquids ($\mu_l \lesssim 0.01$ Pa·s), bubble neck first shows the local elongation before pinch-off, which is consistent with the results in reference (Gordillo 2008). The radius of bubble neck gradually decreases during the whole pinch-off process, the bubble neck converges to a point, and finally it suddenly breaks (see Fig. 8 for details). Reference (Burton et al. 2005) attributes this sudden fracture to inherent Kelvin–Helmholtz instability in dynamics. After the neck pinch-off, the upper and lower parts show an internal concavity, similar to the results of reference (Burton et al. 2005). Reference (Burton et al. 2005) observed a minimum radius of $R_{min} = 25$ μm for sudden neck rupture at a frame rate of 100 000 fps, but reference (Thoroddsen et al. 2007) did not observe sudden rupture at a frame rate of 200 000 fps. The authors observed a minimum radius of about $R_{min} = 7$ μm for sudden neck rupture at 1 μs error (at $\mu_l = 0.001$ Pa·s). This difference may be from the low temporal resolution in the reference. In addition, the present results do not show the phenomenon of " the apexes of the upper and lower conical parts flatten after pinch-off" as described in Jiang et al. (2017) and (Thoroddsen et al. 2007), because the experimentally observed flat top edge of gas cones is only the projection of the end of a bubble (Thoroddsen et al. 2007).

## Neck Profile Shape of Each Viscosity Before Neck Pinch-off

In order to further study the dynamics of the pinch-off process, the process of neck pinch-off under different viscosities was first observed. Figure 4 demonstrates the evolution of the contour line of bubble neck before bubble pinch-off in liquids of $\mu_l = 0.005$, 0.08 and 0.2 Pa·s. The arrow shows the direction of advance in time. The innermost curves are the contour lines closest to pinch-off, and all contour lines do not overlap as time advances,

Fig. 3 Processes of bubble Pinch-off in liquids of different viscosities (Blue region indicates the gas phase, and red region indicates the liquid phase.)

μ_l/Pa·s	Before neck pinch-off		Neck pinch-off	After neck pinch-off	
0.001	83.059ms	83.266ms	83.270ms	83.273ms	84.369ms
0.005	89.309ms	89.346ms	89.353ms	89.363ms	89.490ms
0.05	130.863ms	130.920ms	130.951ms	131.020ms	131.122ms
0.08	166.423ms	166.503ms	166.570ms	166.632ms	166.714ms
0.1	184.853ms	185.148ms	185.187ms	185.345ms	185.460ms
0.2	255.194ms	255.735ms	255.972ms	256.049ms	256.295ms

i.e., the contour line of bubble neck continues to change. In low-viscosity liquids, the neck profile resembles a pair of symmetrical conical shape. The neck profile does not become slenderer as reported in reference (Thoroddsen et al. 2007), but it is getting closer to a conical shape (i.e., the cone top becomes increasingly pointed). Moreover, the neck position corresponding to the minimum radius is only radially translated (this means that the minimum radius

of bubble neck is decreasing) whereas the axial position remains unchanged. This is similar to the results of references (Thoroddsen et al. 2007) and (Gordillo et al. 2005). In intermediate-viscosity liquids, bubble neck is asymmetric up and down, which does not show a parabolic shape reported in reference (Burton et al. 2005). In high-viscosity liquids, experimental and numerical studies of water droplets pinch-off in silicone oil ($\mu_g/\mu_l \approx 10^{-3}$-$10^{-4}$) were

(a) $\mu_l = 0.005$ Pa·s   (b) $\mu_l = 0.08$ Pa·s   (c) $\mu_l = 0.2$ Pa·s
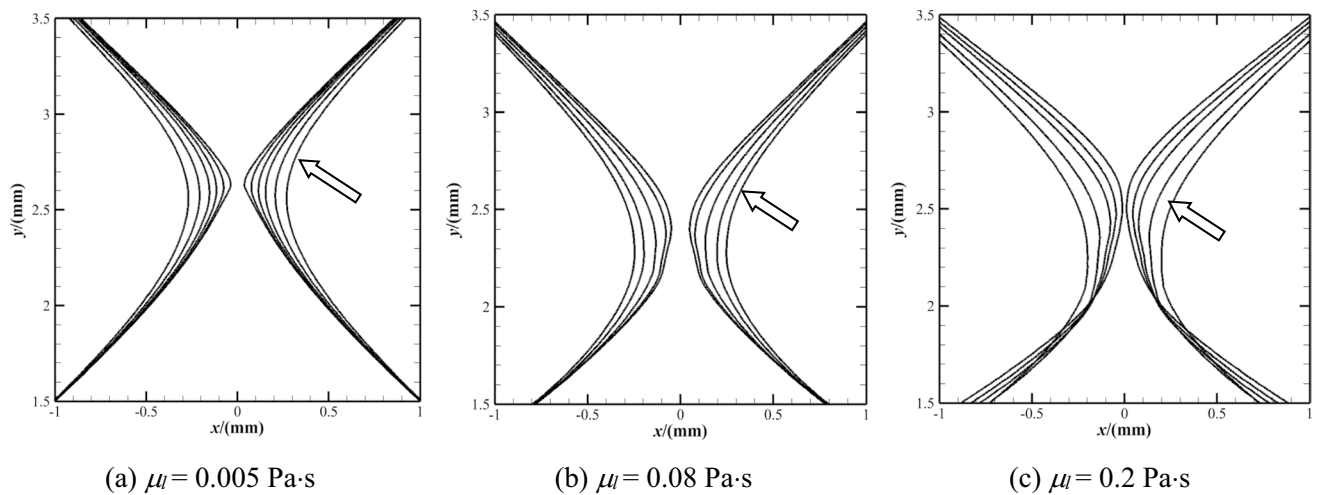
Fig. 4 Evolution of neck profile before bubble pinch-off. (**a**) $\mu_l = 0.005$ Pa·s. (**b**) $\mu_l = 0.08$ Pa·s. (**c**) $\mu_l = 0.2$ Pa·s
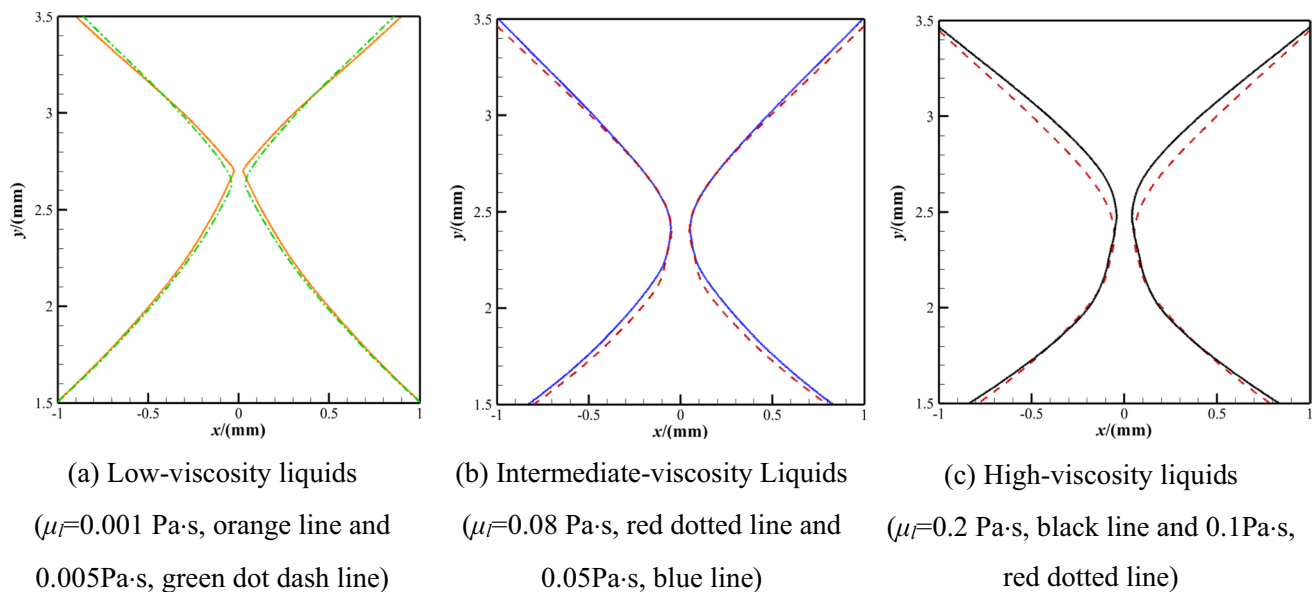
carried out in reference (Suryo et al. 2004), and it was found that the shape of the neck profile does not change as the pinch-off proceeds, but only gradually translates towards the axis. In reference (Thoroddsen et al. 2007), the authors observed experimentally that the neck profile becomes sharper and sharper, and it moves only along the axial direction. Obviously, the present phenomenon is different from that of references. The current study also fails to overlap the contour lines of bubble neck at the viscosity ratio $\mu_g/\mu_l \approx 8.9 \times 10^{-5}$, which indicates a continuous change in the shape of bubble neck. This is inconsistent with the results of reference (Suryo et al. 2004). This is because there is a difference between droplet pinch-off and bubble pinch-off. Moreover, the location of pinch-off point is gradually shifted upwards along the axial direction and the contour of the lower part of bubble neck is not smooth. This is not consistent with the results of reference (Thoroddsen et al. 2007). This may be due to the fact that a more viscous liquid ($\mu_l = 3.5$ Pa·s) is used in the experiment for the convenience of observation in reference (Longuet-Higgins et al. 1991), and the large viscous force suppresses the rising effect due to buoyancy during pinch-off. As pointed out by Longuet-Higgins et al. (Longuet-Higgins et al. 1991), bubble neck becomes unstable at the later stage of pinch-off, the neck contour line is not exactly hyperbolic, and thus the contour of the lower part of bubble neck is not smooth.

Figure 5 compares the neck contour at $R_{min} = 50$ µm during bubble pinch-off in the liquids of $\mu_l = 0.005$, 0.08 and 0.2 Pa·s. It can be seen that the pinch-off point is highest in the low-viscosity liquid. As the liquid-phase viscosity increases, bubble neck becomes slenderer. This is similar to the results of Thoroddsen et al. (Thoroddsen et al. 2007).
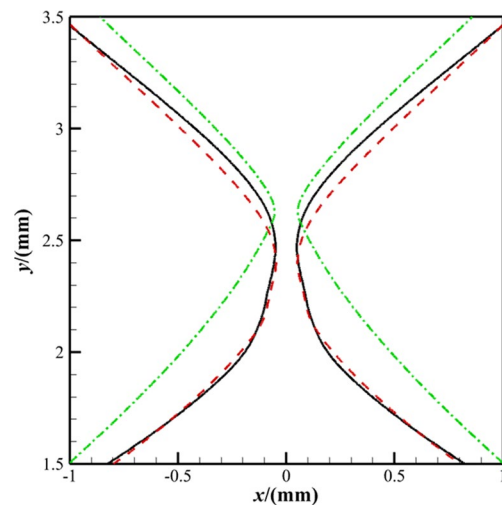
Fig. 5 Bubble neck profiles at $R_{min} = 50$ µm in liquids ($\mu_l = 0.005$ Pa·s, green dot dash line; $\mu_l = 0.08$ Pa·s, red dot dash line; and $\mu_l = 0.2$ Pa·s, black line)

Figure 6 shows the contour of bubble neck in the same liquid viscosity range at $R_{min} = 50$ µm. It can be seen that the contour lines of bubble neck do not overlap even in the same range of liquid viscosity. Figures 6(a) and 6(b) show the contour of bubble neck in low and intermediate viscosity liquids, and they show that even a small change in liquid viscosity can cause a significant change in the axial position of the neck contour due to the relatively small viscous resistance. Figure 6(c) shows the contour of bubble neck in high-viscosity liquids, in which the change in liquid-phase viscosity fails to cause the change in the axial position of the neck contour due to the relatively large viscous resistance. Instead, the larger the liquid-phase viscosity is, the longer the neck becomes in the axial direction.

(a) Low-viscosity liquids

(μ_l=0.001 Pa·s, orange line and

0.005Pa·s, green dot dash line)

(b) Intermediate-viscosity Liquids

(μ_l=0.08 Pa·s, red dotted line and

0.05Pa·s, blue line)

(c) High-viscosity liquids

(μ_l=0.2 Pa·s, black line and 0.1Pa·s,

red dotted line)

Fig. 6 Profiles of bubble neck with a minimum radius of 50 µm. (**a**) Low-viscosity liquids (μ_l=0.001 Pa·s, orange line and 0.005 Pa·s, green dot dash line). (**b**) Intermediate-viscosity Liquids (μ_l=0.08 Pa·s, red dotted line and 0.05 Pa·s, blue line). (**c**) High-viscosity liquids (μl =0.2 Pa·s,black line and 0.1 Pa·s, red dotted line)
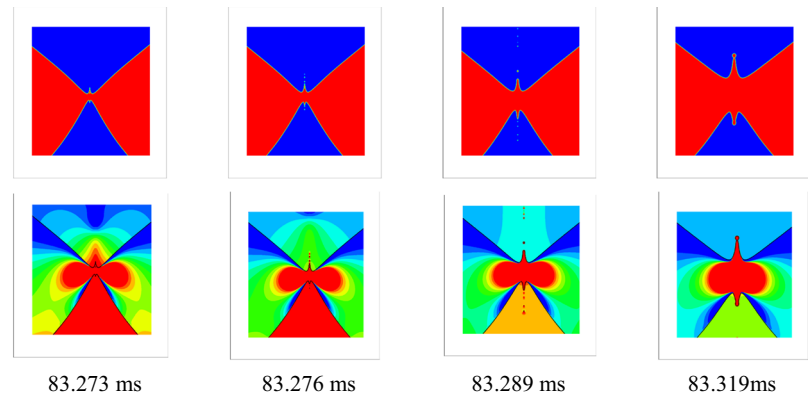
Jet Phenomena in Low-Viscosity Liquids After Neck Pinch-off

In order to further study the dynamic cause of jet generated in the pinch-off process, the jet phenomenon is carefully analyzed. In low-viscosity liquids ($\mu_l \lesssim 0.01$ Pa·s), another typical feature during the neck pinch-off process is the emergence of the high-velocity Worthington jet (Bergmann et al. 2006). Bubble pinch-off is accompanied by the emergence of a strong axial jet, with the external liquid being ejected upwards and downwards into the fractured bubble and into the bubble attached to the needle top, respectively. Bolaños-Jiménez et al. (Bolaños-Jiménez et al. 2008) experimentally found some of the characteristics of the jet, but the details of the jet cannot be presented because the experimental equipment does not allow the observation of the interior of the bubble. Here, on the basis of Fig. 3 and 7 shows the details of the jet phenomenon during the neck pinch-off process in low-viscosity liquids (μ_l = 0.001 and 0.005 Pa·s).
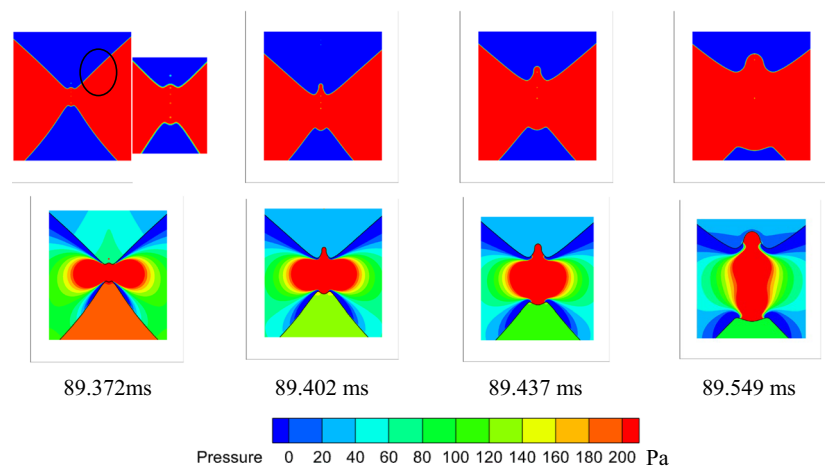
As shown in Figs. 7(a) and 7(b), after the neck pinch-off in the liquids of μ_l = 0.001 and 0.005 Pa·s, a jet occurs, satellite bubbles enter into the gas cone along with jets in the top and bottom directions, causing the cone top to be concave inwards. This is due to the fact that in low-viscosity liquids, when the liquid near the bubble neck converges to the neck, it induces radial collapse under the liquid pressure (Lohse et al. 2004). This results in a sudden fracture of the neck at a very high velocity, and then the liquid rapidly converges to

the pinch-off neck in an axisymmetric manner. Due to the incompressibility of liquid, the liquid, which converges in the region of the neck, flows upwards and downwards along the axis in the form of jets. At the same time, the inertial aggregation of the liquid phase generates a large pressure peak that pushes satellite bubbles upwards into the bubble and downwards into the needle part along the axis (Thoroddsen and Shen 2001). As described in reference (Longuet-Higgins et al. 1991), the jets appear due to the continuity of mass and are used to compensate for the incoming flow in the axial direction. In the same range of liquid viscosities, the depth of depression at the top of the cone is smaller for the more viscous liquid μ_l = 0.005 Pa·s, and the jet is weak. The jets do not occur in liquids, of which viscosity is in the medium and high range. This may be due to the fact that the larger liquid-phase viscosity leads to the larger viscous force, and the larger viscous force has the stronger inhibition of the jet. Figure 7(c) demonstrates the pressure distribution along the radial direction near the bubble neck. The three lines in the figure correspond to the position of the top of the lower bubble cone, the middle position between two gas cones, and the position of the top of the upper bubble cone, respectively. It can be seen from Fig. 7(c) that there is a significant difference between the internal pressure of the upper and lower gas cones and the external liquid pressure. The pressure is higher inside the gas cones. The liquid pressure in the middle between two air cones is significantly higher than the pressure in the other parts, thus causing jets along the axis.
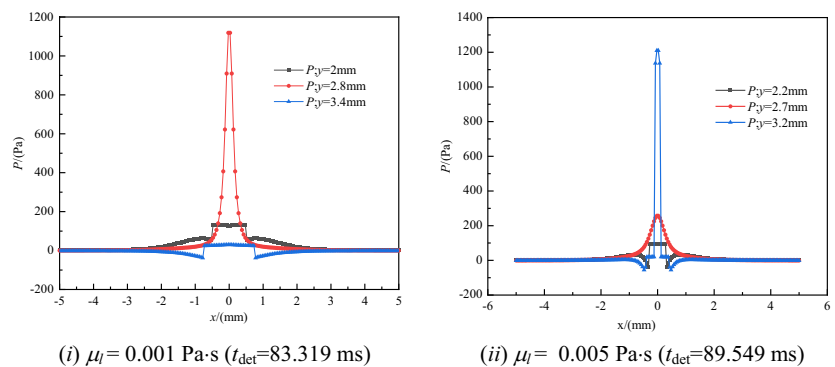
Fig. 7 Jet accompanied by neck pinch-off in low-viscosity liquids. (**a**) Generation process of Worthington jet and corresponding static pressure contour at $\mu_l = 0.001$ Pa·s. (**b**) Generation process of Worthington jet and corresponding static pressure contour at $\mu_l = 0.005$ Pa·s. (**c**) Pressure distribution along the radial direction near bubble neck

83.273 ms   83.276 ms   83.289 ms   83.319ms

(a) Generation process of Worthington jet and corresponding static pressure contour at μ_l=0.001 Pa·s

89.372ms   89.402 ms   89.437 ms   89.549 ms

Pressure   0   20   40   60   80 100 120 140 160 180 200   Pa

(b) Generation process of Worthington jet and corresponding static pressure contour at μ_l=0.005 Pa·s

(*i*) μ_l = 0.001 Pa·s (t_{det}=83.319 ms)   (*ii*) μ_l = 0.005 Pa·s (t_{det}=89.549 ms)

(c) Pressure distribution along the radial direction near bubble neck

Satellite Bubbles of Various Viscosity After Neck Pinch-off

In order to further study the formation reasons of satellite bubbles during the pinch-off process, the formation of satellite bubbles is analyzed. The descriptions about the number, size and distribut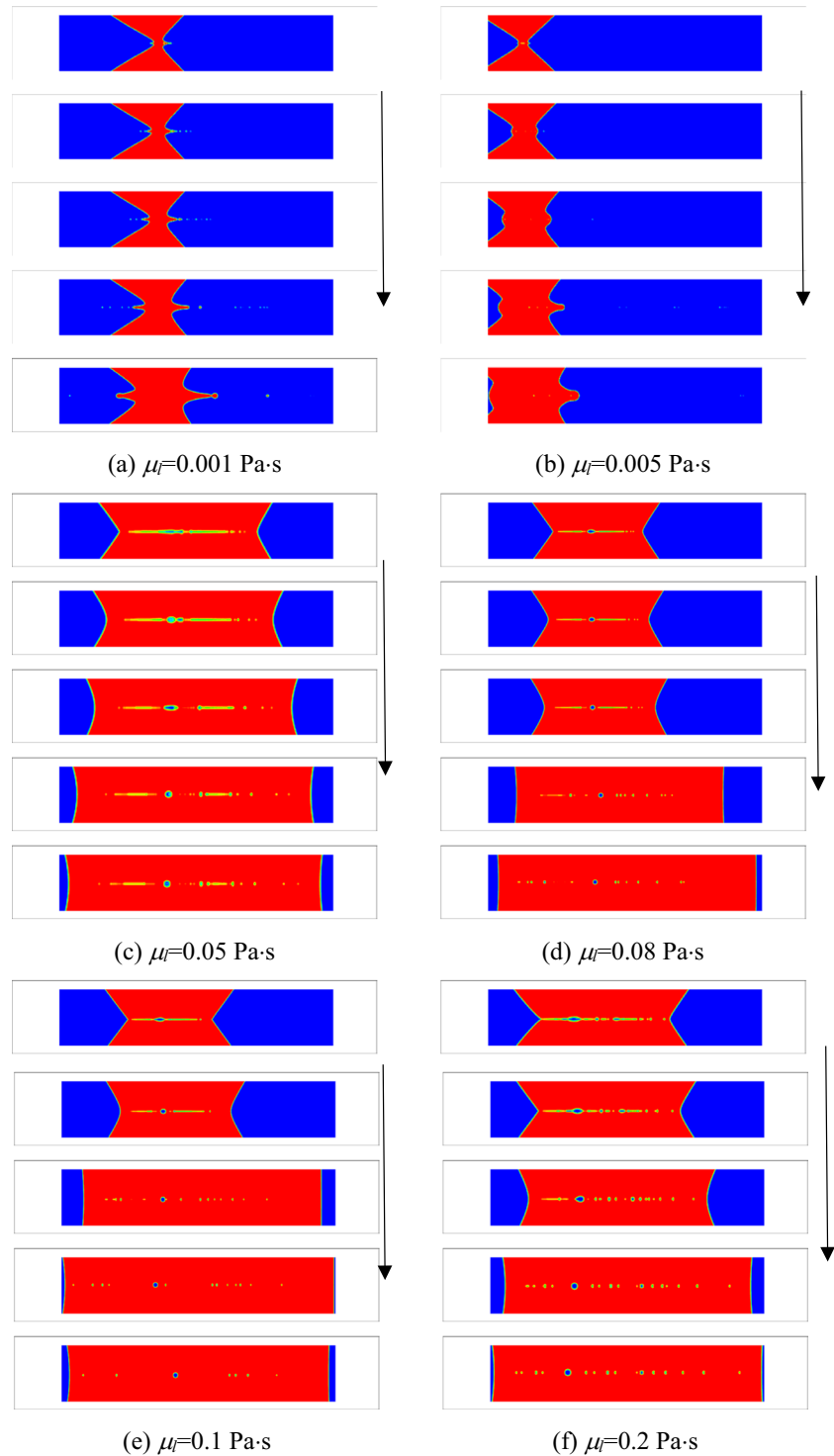ion of satellite bubbles are different after bubble pinch-off. In low-viscosity liquids, Burton et al. (Burton et al. 2005) observed two satellite bubbles with a diameter of 10 μm distributed radially. However, Thoroddsen et al. (Thoroddsen et al. 2007) observed only one satellite bubble in water, and two vertically distributed satellite bubbles were observed in glycerol of μ_l = 0.0078 Pa•s. Figure 5 shows the distribution of satellite bubbles in the liquid with

different viscosity after neck pinch-off in the current study, and the arrow direction shows the formation process of satellite bubbles.

Figures 8(a) and 8(b) show the formation process of satellite bubbles in the low − viscosity liquid. It can be seen that in the liquid of $\mu_l = 0.001$ Pa·s, a small and slender satellite bubble is first observed after the sudden rupture of bubble neck, and then

it is split into six satellite bubbles by two upward and downward jets of liquid. These satellite bubbles flow quickly into the interior of the upper and lower bubbles, respectively. In addition, a small amount of liquid flows into the upper bubble, and thus a new satellite bubble form. Finally, seven satellite bubbles of different sizes are observed. The maximum diameter of satellite bubbles is approximately 9 µm. In addition, four

Fig.8 The formation process of satellite bubble after pinch-off (Rotate all subgraphs counterclockwise by 90°). (**a**) $\mu_l = 0.001$ Pa·s. (**b**) $\mu_l = 0.005$ Pa·s. (**c**) $\mu_l = 0.05$ Pa·s. (**d**) $\mu_l = 0.08$ Pa·s. (**e**) $\mu_l = 0.1$ Pa·s. (**f**) $\mu_l = 0.2$ Pa·s

(a) μ_l=0.001 Pa·s

(b) μ_l=0.005 Pa·s

(c) μ_l=0.05 Pa·s

(d) μ_l=0.08 Pa·s

(e) μ_l=0.1 Pa·s

(f) μ_l=0.2 Pa·s

satellite bubbles with similar size are observed inside the new bubble attached to the needle top. When $\mu_l = 0.005$ Pa·s, about 9 tiny satellite bubbles are observed inside the upper bubble. These satellite bubbles are all vertically distributed, similar to the results of Thoroddsen et al. (Thoroddsen et al. 2007). In references, due to the experimental limitation (unable to observe satellite bubbles into the interior of the bubble), the number of satellite bubbles may be small.

As shown in Figs. 8(c) and 8(d), in the liquids of $\mu_l = 0.05$ and 0.08 Pa·s, a long gas line, which is thick in the middle and thin on both sides, appears between the upper and lower bubbles. As the bubbles gradually separate from the gas line, the gas line begins to rupture from both ends. Due to the continuous squeezing effect of liquid, the mother gas line in the central region is continuously stretched, and it breaks into several short gas lines. Finally, these short gas lines appear as 15 satellite bubbles of different sizes due to surface tension. In the liquids of $\mu_l = 0.1$ and 0.2 Pa·s, as shown in Figs. 8(e) and 8(f), the process is similar to that in intermediate−viscosity liquids. Finally, the gas line is stretched to form about 17 satellite bubbles of different sizes. Satellite bubbles are always vertically distributed as they rise and split. For the current study, the number of satellite bubbles in intermediate- and high-viscosity liquids is slightly less than that observed in reference (Thoroddsen et al. 2007). This may be due to the fact that satellite bubbles continue to split or merge while they rise.

Minimum Radius of Bubble Neck against Time

For the hydrodynamic study of singularity, there are two main configurations: the pinch-off of droplets (Leppinen and Lister 2003; Doshi et al. 2003) and the pinch-off of bubbles generated from a vertical needle (Burton et al. 2005). The neck pinch-off of the two configurations is controlled by different dynamics. The pinch-off of droplets is caused due to the contraction of surface tension, whereas the pinch-off of bubbles is controlled by the inertia of fluids (Thoroddsen et al. 2008). The process of bubble pinch-off in Newtonian liquids is usually quantified with the evolution of R_{min} versus time (Jiang et al. 2017). A model proposed by Longuet-Higgins et al. (Longuet-Higgins et al. 1991) shows that R_{min} decreases with time in a power−law manner. This is essentially a kinematic model, which is formulated using a sink of constant strength Q on the axis of symmetry.

$$u = \frac{dR_{min}}{dt} = \frac{-Q}{2\pi R_{min}} \Rightarrow \frac{d}{dt}(R^2_{min}) = \frac{-Q}{\pi} \qquad (10)$$
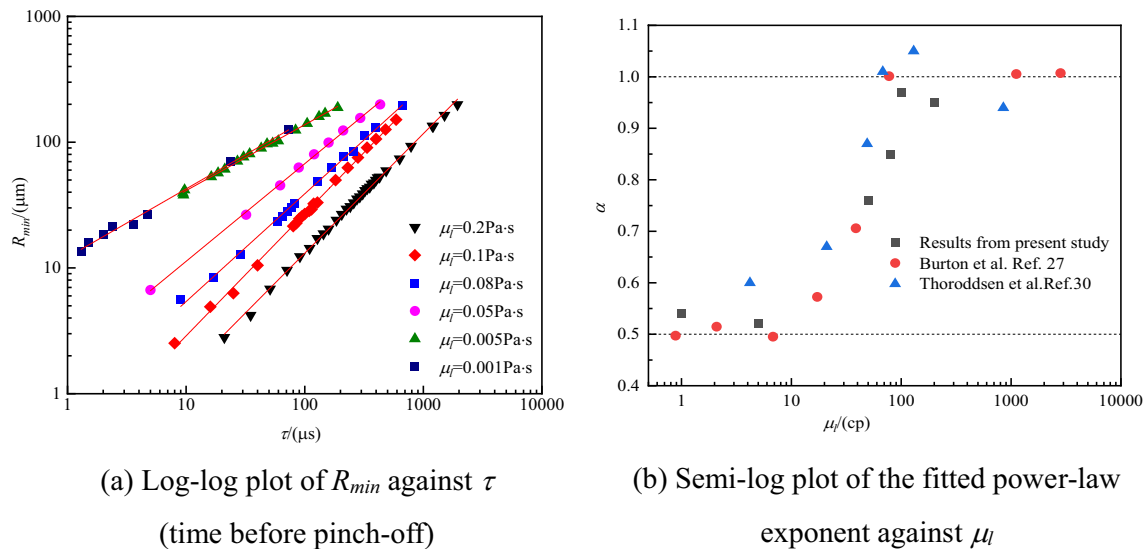
which has the solution

$$R_{min} \propto (t_0 - t)^\alpha$$

According to the above theoretical model, in a relatively short period of time before pinch-off, the relationship between R_{min} and time is $R_{min}(t) \propto A(\tau)^\alpha$. $\tau = (t_c\text{-}t)$ denotes the interval between any an instantaneous moment t and the pinch-off moment t_c during the pinch-off process (Thoroddsen et al. 2007).

For the current calculation results, the data of $R_{min} \leq 200$ μm is used to analyze according to reference (Burton et al. 2005), and it is found that the relationship between the power−law exponent and time follows the power−law manner of the model, as shown in Fig. 9(a). Data ($R_{min} \leq 200$ μm) are selected according to reference (Burton et al. 2005), and the power-law exponent α is fitted with a power-law function ($R_{min} = A\tau^\alpha$). t_c is selected with reference to reference (Burton et al. 2005). The intermediate time between the current time of the neck connection and the next time of the neck pinch-off is selected as t_c in low-viscosity liquids, with an error of about ± 5 μs. In intermediate-viscosity liquids, the flow time at a constant neck radius is selected as the pinch-off time (t_c), since the flow after this point is determined by different dynamics (Doshi et al. 2003). In high-viscosity liquids, t_c is chosen to be the point at which the two cusps separate. In viscous liquids, the exact time of pinch-off is not easily recognizable due to the elongation of bubble neck, and thus the selection may result in errors. That has a slight effect on the power-law index α. Figure 9(a) shows R_{min} against τ before the neck pinch-off in a double logarithmic coordinate system. It can be seen that for all liquids, the relationship between R_{min} and τ complies with the equation of $R_{min} = A\tau^\alpha$. α increases with an increase in liquid-phase viscosity, and it tends to 1 approximately. In low-viscosity liquids ($\mu_l = 0.001$ and 0.005 Pa·s), the fitted values of power-law exponents are $\alpha \approx 0.54$ and 0.52, respectively. There is a small difference from the results of reference (Burton et al. 2005). This may be due to the fact that the frame rate is within 100 000 fps in experiments, making it difficult determine the exact pinch-off point. In highly viscous liquids ($\mu_l = 0.1$ and 0.2 Pa·s), the minimum radius follows $R_{min} = (\sigma/2 \mu_l)\tau$ (Burton et al. 2005). The fitted values of power-law exponents are $\alpha \approx 0.97$ and 0.95, respectively; and they are similar to the results of reference (Thoroddsen et al. 2007). The coefficient $A \approx 0.164$ is slightly larger than the value $\sigma/2 \mu_l = 0.1625$. Similar discrepancies were also reported by Burton et al. (Burton et al. 2005; Rajesh et al. 2022). In intermediate-viscosity liquids ($\mu_l = 0.05$ and 0.08 Pa·s), the values of the power-law exponent are $\alpha \approx 0.76$ and 0.85, respectively.

To investigate the relationship between α and μ_l, the variation of α with μ_l is plotted in Fig. 9(b). Experimental data from references (Burton et al. 2005) and (Thoroddsen et al. 2007) are also plotted Fig. 9(b). It can be seen that the present values of α are in better agreement with the experimental results in references (Burton et al. 2005; Thoroddsen et al. 2007). α increases as the liquid-phase viscosity increases from 0.005 Pa·s to 0.1 Pa·s. However, for the present results,

(a) Log-log plot of R_{min} against τ

(time before pinch-off)

(b) Semi-log plot of the fitted power-law

exponent against μ_l

Fig. 9 The minimum radius of bubble neck against time and liquid viscosity. (**a**) Log–log plot of R_{min} against τ (time before pinch-off). (**b**) Semi-log plot of the fitted power-law exponent against μ_l

α is slightly greater than 0.5 when $\mu_l = 0.001$ Pa·s and it is slightly less than 1 when $\mu_l = 0.2$ Pa·s. The results of reference (Thoroddsen et al. 2007) show a similar trend.

Kinetic Analysis of Neck Pinch-off

The flow field around the bubble, especially near the gas–liquid interface, can explain the contribution of the liquid-phase flow to bubble pinch-off. Therefore, the flow field is analyzed first. Figure 10(a) shows the flow field for the liquids of $\mu_l = 0.001$, 0.08 and 0.2 Pa·s at time corresponding to $R_{min} = 600$, 400, 200 μm and after the pinch-off. As shown in Fig. 10, with the growth of a bubble and the formation of bubble neck before pinch-off, the liquid exactly above the bubble flows upwards and then flows downwards through the sides of the bubble to the bubble neck, forming a radial flow in the vicinity of the bubble neck. This is similar to the experimental results of reference (Thoroddsen et al. 2007). Under certain conditions, vortices appear inside the bubble. Because the shape of the bubble neck inside the bubble is similar to a diffuser, flow separation may occur as the gas flows through the neck. Prior to pinch-off, the diffuser-like bubble neck has a small cone angle, so the flow separation does not occur. However, as the pinch-off proceeds, the bubble neck taper angle is close to 45°, and thus the flow separation occurs. In the pinch-off, the bubble is pushed upwards, and the motion of the liquid near the pinch-off point is the combination of strong axial and slight radial motions. This is consistent with the particle motion experimentally observed in reference (Thoroddsen et al. 2007) and the theoretical description in reference (Gordillo 2008)

(a smooth transition from the purely inward radial flow to the straining flow with a stagnation-point structure). As shown in Fig. 10, the flow of liquid around the bubble plays an important role in bubble pinch-off. Then, to quantitatively analyze the magnitude of the liquid-phase velocity at the bubble neck position, the liquid-velocity along the radial direction at $R_{min} = 500$ μm is shown in Fig. 10(b). It can be seen that for all viscosities, the closer to the bubble neck is, the greater the liquid velocity is. This means that the bubble neck is much affected by the dynamic pressure of the liquid phase. And the less viscous the liquid phase is, the greater its velocity is, and the more the neck is much affected by the dynamic pressure of the liquid phase. So, the liquid-phase viscosity is different, the liquid-phase velocity around the bubble is different, and thus the phenomena of bubble pinch-off is also different. Finally, obtaining the liquid pressure distribution around the bubble neck is of great significance in understanding the mechanism of bubble pinch-off. The pressure values (gauge pressure) at $R_{min} = 400$ μm are presented in Fig. 11. It can be seen that in the region away from the bubble neck, the liquid pressure remains constant; and in the region adjacent to the bubble neck, the value of the liquid pressure suddenly becomes very small. The pressure difference between these two regions is the main cause for the radial flow of liquids. As stated in reference (Bolaños-Jiménez et al. 2008), the radial acceleration of liquids during bubble pinch-off is driven by the radial difference in the pressure of liquids. It is also observed that as the liquid viscosity increases, the pressure difference becomes smaller and smaller. This results in a longer time required for bubble pinch-off in highly viscous liquids.
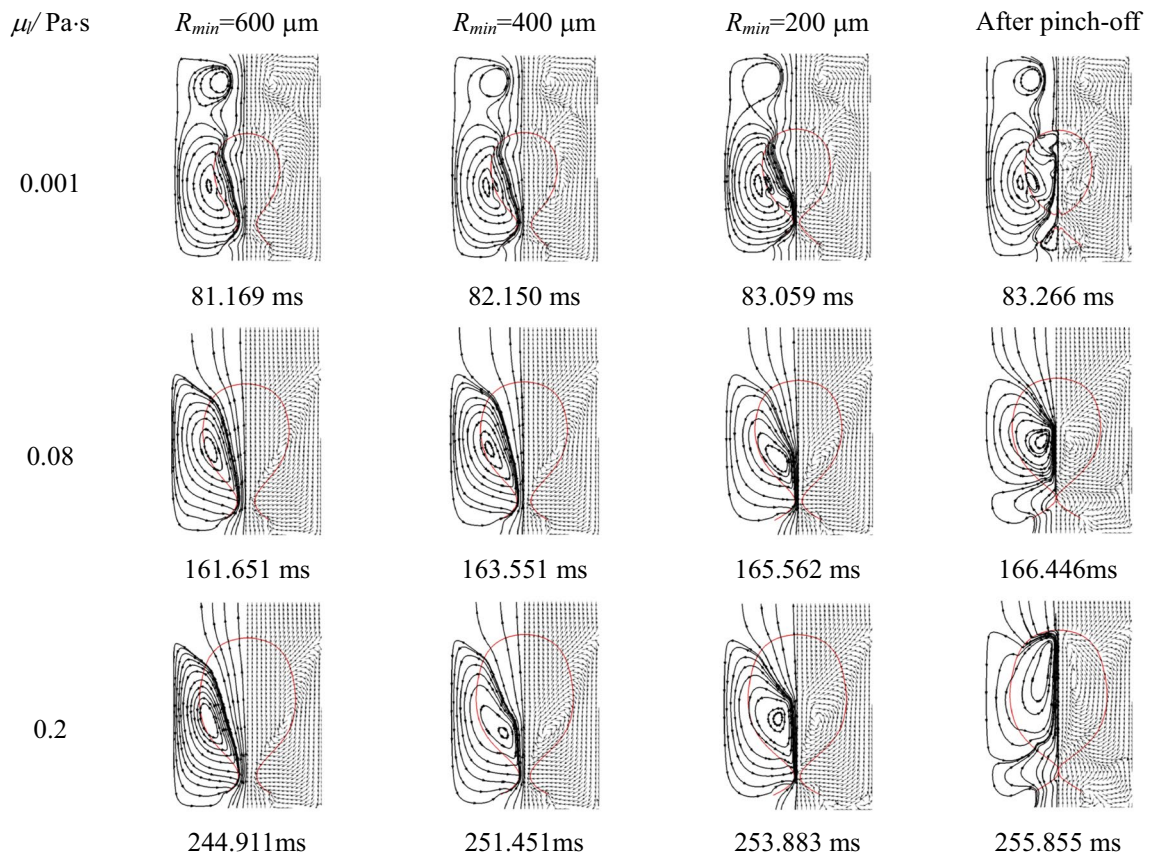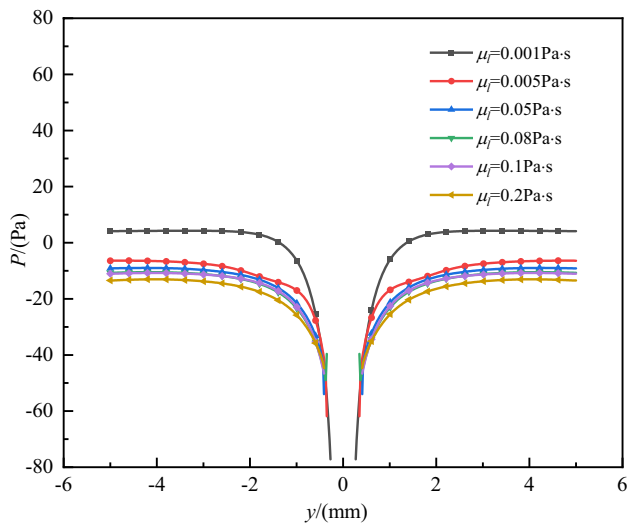
(a) Flow field during bubble pinch-off
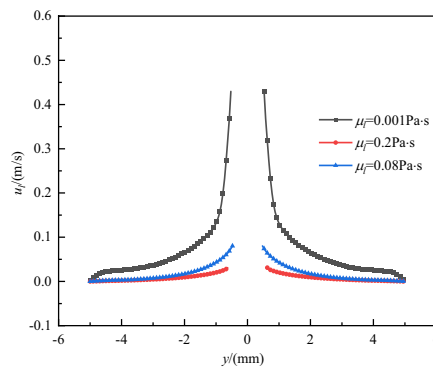
(b) Liquid-phase velocity along the radial direction at the position of R_{min}=400 μm

Fig. 10 Flow field and liquid velocity distribution during bubble pinch-off. (**a**) Flow field during bubble pinch-off. (**b**) Liquid-phase velocity along the radial direction at the position of R_{min} = 400 μm

Therefore, combined with the above comprehensive analysis of the flow field, liquid velocity and liquid pressure near the neck pinch, the pinch dynamic analysis can be roughly obtained. First, during the growth process of bubbles, the curvature of the local interface of bubbles near the needle tube tends to zero as the bubble grows. This leads to the fact that the capillary pressure (σ/r) tends to zero at the local interface. Thus, the original pressure balance inside and outside

the bubble cannot be maintained. The liquid pressure outside the bubble is greater than the gas pressure inside the bubble. The liquid outside the bubble can push the local interface to move inward. Bubble neck begins to form. Second, it can be seen that the bubble growth pushes the liquid above it to flow diagonally upwards first and then downwards, forming an annular flow. The resulting dynamic pressure promotes the formation of bubble neck. Since the resistance to bubble

Fig. 11 Distribution of liquid-phase static pressure along the radial direction (Gauge pressure) at the position of $R_{min} = 400$ μm

Conclusions

In this paper, bubble pinch-off in liquids of different viscosities was investigated by the numerical method. The contour shape of bubble neck, the jet that occurs in low-viscosity liquids, as well as the distribution and number of satellite bubbles after neck pinch-off in intermediate- and high-viscosity liquids are analyzed, and the relationship between the minimum neck radius (R_{min}) and the pinch-off time (τ) is fitted with a power-law function. The following conclusions can be drawn:

(1) In low−viscosity liquids, the process of bubble pinch−off is relatively fast, and satellite bubbles during bubble pinch−off show vertical distribution, which enter the upper and lower parts with the jet after bubble pinch−off.
(2) In low−viscosity liquids, the position of R_{min} only moves along the radial direction and does not move along the axial direction; however, in intermediate− and high−viscosity liquids, the position of R_{min} moves along the radial and axial directions.
(3) For all viscosity liquids, R_{min} against time follows the equation of $R_{min} = A\tau^{\alpha}$. The power law exponent (α) increases with an increase in liquid−phase viscosity, and it increases from 0.52 for low−viscosity liquids to 1 for high−viscosity fluids.
(4) The formation of bubble neck and pinch−off are caused by following three phenomena: a great decrease in the curvature of bubble local interface, the formation of an annular flow, and the Bernoulli effect.

Author Contributions The authors confirm their contribution to the paper as follows: study conception and design: Meng Jia, Mingjun Pang; data collection: Meng Jia; analysis and interpretation of results: Meng Jia, Mingjun Pang; draft manuscript preparation: Meng Jia. All authors reviewed the results and approved the final version of the manuscript.

Data Availability No datasets were generated or analysed during the current study.

Declarations

Ethical Approval Not applicable.

Consent to Participate Not applicable.

growth in low−viscosity liquids is smaller than that in intermediate−and high−viscosity liquids, the bubbles grow faster in low−viscosity liquids. The liquid above the bubble flows downwards at a relatively high rate. And in low−viscosity liquids, the viscous dissipation is small. The liquid impacts the lower part of the bubble at a high rate, resulting in the formation of bubble neck. In addition, the Bernoulli effect causes a decrease in the pressure at the neck position inside the bubble when the gas flows through the bubble neck at a high rate. The liquid pressure near bubble neck also decreases due to $p_l = p_g - \sigma/r_o$. Thus, the resulting favorable pressure gradient accelerates the liquid to flow toward bubble neck along both radial and axial directions(Gordillo et al. 2005), which in turn promotes the formation of bubble neck. Finally, according to the principles of conservation of mass and momentum, the flow area in bubble neck is smaller so the gas−phase velocity is higher, and the pressure is lower in the neck region. When the pressure outside the bubble is greater than the pressure exactly near bubble neck, bubble neck will break. And in low−viscosity liquids, an overall tear occurs when bubble neck breaks because of the high velocity of the gas in bubble neck (the large inertia) and the low viscosity of liquid (the low viscous resistance). In intermediate−and high−viscosity liquids, the bubble growth is slow due to a large viscous resistance, resulting in a smaller flow rate of liquid and a longer time required for the neck formation. Under the influence of the large viscous resistance, the dynamic pressure of the fluids in bubble neck, and the buoyancy force, bubble neck slowly becomes thin and is gradually elongated to form a gas line. And eventually it breaks.

Conflicts of Interest The authors declare that they have no conflicts of interest to report regarding the present study.

Competing interests The authors declare no competing interests

References

Albadawi, A., Donoghue, D.B., Robinson, A.J., Murray, D.B., Delauré, Y.M.C.: Influence of surface tension implementation in volume of fluid and coupled volume of fluid with level set methods for bubble growth and detachment. Int. J. Multiph. Flow **53**, 11–28 (2013). https://doi.org/10.1016/j.ijmultiphaseflow.2013.01.005

Bergmann, R., van der Meer, D., Stijnman, M., Sandtke, M., Prosperetti, A., Lohse, D.: Giant bubble pinch-off. Phys. Rev. Lett. **96**(15), 154505 (2006). https://doi.org/10.1103/PhysRevLett.96.154505

Bolaños-Jiménez, R., Sevilla, A., Martínez-Bazán, C., Gordillo, J.M.: Axisymmetric bubble collapse in a quiescent liquid pool. II. Experimental Study. Physics of Fluids **20**(11), 112104 (2008). https://doi.org/10.1063/1.3009298

Bolanos-Jiménez, R., Sevilla, A., Martínez-Bazán, C., van der Meer, D., Gordillo, J.M.: The effect of liquid viscosity on bubble pinch-off. Phys. Fluids **21**(7), 072103 (2009). https://doi.org/10.1063/1.3173195

Burton, J.C., Waldrep, R., Taborek, P.: Scaling and instabilities in bubble pinch-off. Phys. Rev. Lett. **94**(18), 184502 (2005). https://doi.org/10.1103/PhysRevLett.94.184502

Chandrasekhar, S.: Principles of stellar dynamics. Courier Corporation, Massachusetts (2005)

Chen, Y.J., Steen, P.H.: Dynamics of inviscid capillary breakup: collapse and pinchoff of a film bridge. J. Fluid Mech. **341**, 245–267 (1997). https://doi.org/10.1017/S002211209700548X

Chu, P., Finch, J., Bournival, G., Ata, S., Hamlett, C.: A review of bubble break-up. Adv. Coll. Interface. Sci. **270**, 108–122 (2019). https://doi.org/10.1016/j.cis.2019.05.010

Di Bari, S., Lakehal, D., Robinson, A.J.: A numerical study of quasi-static gas injected bubble growth: Some aspects of gravity. Int. J. Heat Mass Transf. **64**, 468–482 (2013). https://doi.org/10.1016/j.ijheatmasstransfer.2013.04.002

Doshi, P., Suryo, R., Yildirim, O.E., McKinley, G.H., Basaran, O.A.: Scaling in pinch-off of generalized Newtonian fluids. J. Nonnewton. Fluid Mech. **113**(1), 1–27 (2003). https://doi.org/10.1016/S0377-0257(03)00081-8

Eggers, J.: Universal pinching of 3D axisymmetric free-surface flow. Phys. Rev. Lett. **71**(21), 3458 (1993). https://doi.org/10.1103/PhysRevLett.71.3458

Eggers, J.: Nonlinear dynamics and breakup of free-surface flows. Rev. Mod. Phys. **69**(3), 865 (1997). https://doi.org/10.1103/RevModPhys.69.865

Eggers, J., Fontelos, M.A., Leppinen, D., Snoeijer, J.H.: Theory of the collapsing axisymmetric cavity. Phys. Rev. Lett. **98**(9), 094502 (2007). https://doi.org/10.1103/PhysRevLett.98.094502

García-Magariño, A., Lopez-Gavilan, P., Sor, S., Terroba, F.: Micro/Bubble drag reduction focused on new applications. J. Marine Sci. Eng. **11**(7), 1315 (2023). https://doi.org/10.3390/jmse11071315

Garzon, M., Gray, L.J., Sethian, J.: Droplet and bubble pinch-off computations using level sets. J. Comput. Appl. Math. **236**(12), 3034–3041 (2012). https://doi.org/10.1016/j.cam.2011.03.032

Gordillo, J.M., Fontelos, M.A.: Satellites in the inviscid breakup of bubbles. Phys. Rev. Lett. **98**(14), 144503 (2007). https://doi.org/10.1103/PhysRevLett.98.144503

Gordillo, J.M., Sevilla, A., Rodríguez-Rodríguez, J., Martínez-Bazán, C.: Axisymmetric bubble pinch-off at high Reynolds numbers. Phys. Rev. Lett. **95**(19), 194501 (2005). https://doi.org/10.1103/PhysRevLett.95.194501

Gordillo J M. Axisymmetric bubble collapse in a quiescent liquid pool. I. Theory and numerical simulations. Physics of Fluids 20(11):112103 (2008). https://doi.org/10.1103/PhysRevLett.98.094502

Han, W., Chen, X.: Effect of geometry configuration on the merged droplet formation in a double T-junction. Microgravity Sci. Technol. **31**(6), 855–864 (2019). https://doi.org/10.1007/s12217-019-09720-y

Han, W., Chen, X.: A review: Applications of ion transport in micro-nanofluidic systems based on ion concentration polarization. J. Chem. Technol. Biotechnol. **95**(6), 1622–1631 (2020). https://doi.org/10.1002/jctb.6288

Han, W., Chen, X.: A review on microdroplet generation in microfluidics. J. Braz. Soc. Mech. Sci. Eng. **43**(5), 247 (2021). https://doi.org/10.1007/s40430-021-02971-0

Han, W., Mu, X., Liu, Y., et al.: A critical review of on-line oil wear debris particle detection sensors. J. Marine Sci. Eng. **11**(12), 2363 (2023). https://doi.org/10.3390/jmse11122363

Han, W., Wang, X., Li, W., et al.: Numerical simulation study of bubble breakup mechanism in microchannels with V-shaped obstacle. Chem. Eng. Processing-Process Intensif. **200**, 109791 (2024). https://doi.org/10.1016/j.cep.2024.109791

Jia, M., Pang, M.: Numerical Investigations on Effects of Physical Parameters on Single Bubble Generation from Capillary Needles in Newtonian Liquids. Front. Heat Mass Transf. **21**, 337–366 (2023). https://doi.org/10.32604/fhmt.2023.044286

Jiang, X.F., Zhu, C., Li, H.Z.: Bubble pinch-off in Newtonian and non-Newtonian fluids. Chem. Eng. Sci. **170**, 98–104 (2017). https://doi.org/10.1016/j.ces.2016.12.057

Keim, N.C., Møller, P., Zhang, W.W., Nagel, S.R.: Breakup of air bubbles in water: Memory and breakdown of cylindrical symmetry. Phys. Rev. Lett. **97**(14), 144503 (2006). https://doi.org/10.1103/PhysRevLett.97.144503

Kulkarni, A.A., Joshi, J.B.: Bubble formation and bubble rise velocity in gas− liquid systems: a review. Ind. Eng. Chem. Res. **44**(16), 5873–5931 (2005). https://doi.org/10.1021/ie049131p

Leppinen, D., Lister, J.R.: Capillary pinch-off in inviscid fluids. Phys. Fluids **15**(2), 568–578 (2003). https://doi.org/10.1063/1.1537237

Liebling, S.L., Choptuik, M.W.: Black hole criticality in the Brans-Dicke model. Phys. Rev. Lett. **77**(8), 1424 (1996). https://doi.org/10.1103/PhysRevLett.77.1424

Lister, J.R., Stone, H.A.: Capillary breakup of a viscous thread surrounded by another viscous fluid. Phys. Fluids **10**(11), 2758–2764 (1998). https://doi.org/10.1063/1.869799

Lohse, D., Bergmann, R., Mikkelsen, R., Zeilstra, C., van der Meer, D., Versluis, M., van der Weele, K., van der Hoef, M., Kuipers, H.: Impact on soft sand: void collapse and jet formation. Phys. Rev. Lett. **93**(19), 198003 (2004). https://doi.org/10.1103/PhysRevLett.93.198003

Longuet-Higgins, M.S., Kerman, B.R., Lunde, K.: The release of air bubbles from an underwater nozzle. J. Fluid Mech. **230**, 365–390 (1991). https://doi.org/10.1017/S0022112091000836

López, J., Hernández, J., Gómez, P., Faura, F.: A volume of fluid method based on multidimensional advection and spline interface reconstruction. J. Comput. Phys. **195**(2), 718–742 (2004). https://doi.org/10.1016/j.jcp.2003.10.030

Ma, D., Liu, M., Zu, Y., Tang, C.: Two-dimensional volume of fluid simulation studies on single bubble formation and dynamics in bubble columns. Chem. Eng. Sci. **72**, 61–77 (2012). https://doi.org/10.1016/j.ces.2012.01.013

Oguz, H.N., Prosperetti, A.: Dynamics of bubble growth and detachment from a needle. J. Fluid Mech. **257**, 111–145 (1993). https://doi.org/10.1017/S0022112093003015

Oshaghi, M.R., Afshin, H., Firoozabadi, B.: Investigation of bubble formation and its detachment in shear-thinning liquids at low capillary and Bond numbers. Theoret. Comput. Fluid Dyn. **33**, 463–480 (2019). https://doi.org/10.1007/s00162-019-00502-1

Pahlavan, A.A., Stone, H.A., McKinley, G.H., Juanes, R.: Restoring universality to the pinch-off of a bubble. Proc. Natl. Acad. Sci. **116**(28), 13780–13784 (2019). https://doi.org/10.1073/pnas.1819744116

Parmigiani, A., Faroughi, S., Huber, C., Bachmann, O., Su, Y.: Bubble accumulation and its role in the evolution of magma reservoirs in the upper crust. Nature **532**(7600), 492–495 (2016). https://doi.org/10.1038/nature17401

Plewa, T., Calder, A.C., Lamb, D.Q.: Type Ia supernova explosion: gravitationally confined detonation. Astrophys J **612**(1), L37 (2004). https://doi.org/10.1086/424036

Rajesh, S., Peddada, S.S., Thiévenaz, V., Sauret, A.: Pinch-off of bubbles in a polymer solution. J. Nonnewton. Fluid Mech. **310**, 104921 (2022). https://doi.org/10.1016/j.jnnfm.2022.104921

Rodríguez-Rodríguez, J., Gordillo, J.M., Martínez-Bazán, C.: Breakup time and morphology of drops and bubbles in a high-Reynolds-number flow. J. Fluid Mech. **548**, 69–86 (2006). https://doi.org/10.1017/S002211200500741X

Rubio, J., Souza, M.L., Smith, R.W.: Overview of flotation as a waste-water treatment technique. Miner. Eng. **15**(3), 139–155 (2002). https://doi.org/10.1016/S0892-6875(01)00216-3

Simmons, J.A., Sprittles, J.E., Shikhmurzaev, Y.D.: The formation of a bubble from a submerged orifice. Eur. J. Mech.-B/fluids **53**, 24–36 (2015). https://doi.org/10.1016/j.euromechflu.2015.01.003

Skobelev, N.K.: Delayed fission of atomic nuclei. Journal of Physics: Conference Series. IOP Publishing, 1555(1):012038 (2020). https://doi.org/10.1103/RevModPhys.85.1541

Suryo, R., Doshi, P., Basaran, O.A.: Non-self-similar, linear dynamics during pinch-off of a hollow annular jet. Phys. Fluids **16**(11), 4177–4184 (2004). https://doi.org/10.1063/1.1793631

Temesgen, T., Han, M.: Advancing aerobic digestion efficiency using ultrafine bubbles in wastewater treatment. J. Water Process Eng. **55**, 104072 (2023). https://doi.org/10.1016/j.jwpe.2023.104072

Theander, K., Pugh, R.J.: Surface chemicals concepts of flotation de-inking. Colloids Surf., A **240**(1–3), 111–130 (2004). https://doi.org/10.1016/j.colsurfa.2003.12.014

Thoroddsen, S.T., Shen, A.Q.: Granular jets. Phys. Fluids **13**(1), 4–6 (2001). https://doi.org/10.1063/1.1328359

Thoroddsen, S.T., Etoh, T.G., Takehara, K.: Experiments on bubble pinch-off. Phys. Fluids **19**(4), 042101 (2007). https://doi.org/10.1063/1.2710269

Thoroddsen, S.T., Etoh, T.G., Takehara, K.: High-speed imaging of drops and bubbles. Annu. Rev. Fluid Mech. **40**, 257–285 (2008). https://doi.org/10.1146/annurev.fluid.40.111406.102215

Van Liew, H.D., Hlastala, M.P.: Influence of bubble size and blood perfusion on absorption of gas bubbles in tissues. Respir. Physiol. **7**(1), 111–121 (1969). https://doi.org/10.1016/0034-5687(69)90072-3

Wang, H., Yang, W., Yan, X., Wang, L., Wang, Y.: Regulation of bubble size in flotation: A review. J. Environ. Chem. Eng. **8**(5), 104070 (2020). https://doi.org/10.1016/j.jece.2020.104070

Wang J, Wang G, Zeng Q, Wang Y.: Recent progress on the jetting of single deformed cavitation bubbles near boundaries. J. Hydrodyn. 1–26 (2023). https://doi.org/10.1007/s42241-023-0071-6

Yang, G.Q., Du, B., Fan, L.S.: Bubble formation and dynamics in gas–liquid–solid fluidization—A review. Chem. Eng. Sci. **62**(1–2), 2–27 (2007). https://doi.org/10.1016/j.ces.2006.08.021

Yuan, J., Li, Y., Zhou, Y.: Effect of contact angle on bubble formation at submerged orifices. J. Mater. Sci. **49**, 8084–8094 (2014). https://doi.org/10.1007/s10853-014-8516-5